

Phase diagram of the Su-Schrieffer-Heeger-Hubbard model on a square lattice

Chunhan Feng¹, Bo Xing², Dario Poletti^{2,3}, Richard Scalettar¹ and George Batrouni^{4,5,6,7}

¹Department of Physics, University of California, Davis, California 95616, USA

²Science, Mathematics and Technology Cluster, Singapore University of Technology and Design, 8 Somapah Road, 487372 Singapore

³Engineering Product Development Pillar, Singapore University of Technology and Design, 8 Somapah Road, 487372 Singapore

⁴Université Côte d'Azur, CNRS, Institut de Physique de Nice (INPHYNI), 06000 Nice, France

⁵Centre for Quantum Technologies, National University of Singapore, 2 Science Drive 3 Singapore 117542

⁶Department of Physics, National University of Singapore, 2 Science Drive 3, 117542 Singapore

⁷Beijing Computational Science Research Center, Beijing 100193, China



(Received 6 October 2021; revised 13 July 2022; accepted 14 July 2022; published 18 August 2022)

The Hubbard and Su-Schrieffer-Heeger (SSH) Hamiltonians are iconic models for understanding the qualitative effects of electron-electron and electron-phonon interactions, respectively. In the two-dimensional square lattice Hubbard model at half filling, the on-site Coulomb repulsion U between up and down electrons induces antiferromagnetic (AFM) order and a Mott insulating phase. On the other hand, for the SSH model, there is an AFM phase when the electron-phonon coupling λ is less than a critical value λ_c and a bond order wave when $\lambda > \lambda_c$. In this Letter, we perform numerical studies on the square lattice optical Su-Schrieffer-Heeger-Hubbard Hamiltonian, which combines both interactions. We use the determinant quantum Monte Carlo method which does not suffer from the fermionic sign problem at half filling. We map out the phase diagram and find that it exhibits a direct first-order transition between an antiferromagnetic phase and a bond-ordered wave as λ increases. The AFM phase is characterized by two different regions. At smaller λ the behavior is similar to that of the pure Hubbard model; the other region, while maintaining long-range AFM order, exhibits larger kinetic energies and double occupancy, i.e., larger quantum fluctuations, similar to the AFM phase found in the pure SSH model.

DOI: [10.1103/PhysRevB.106.L081114](https://doi.org/10.1103/PhysRevB.106.L081114)

Introduction. Electron-electron and electron-phonon interactions play important roles in determining the ground state properties of many-body systems. Over the past decades, much computational effort has been put into studying systems that feature one or the other of these interactions. One of the most widely used models to study the effect of an electron-electron interaction with on-site repulsion U is the Hubbard model [1] which exhibits metallic, ferromagnetic, antiferromagnetic (AFM), and superconducting (SC) orders, as well as intricate inhomogeneous spin and charge patterns, depending on U and the doping [2,3]. The physics of the square lattice Hubbard model bears a remarkable resemblance to that of the cuprate superconductors. Two of the most commonly studied electron-phonon Hamiltonians are the Holstein [4] and the Su-Schrieffer-Heeger (SSH) [5] models. Their fundamental difference is that in the former, electrons and phonons interact on a single site, while in the latter, the electron-phonon interactions occur on the bonds, i.e., in the tunneling term. The Holstein interaction is widely used to explore polaron and charge-density-wave (CDW) physics [6–17], and conventional s -wave SC transitions [15,18], while the SSH interaction occurs in systems such as conjugate polymers [19], organic charge transfer salts [20], metal salts [21], and CuGeO₃ [22].

In the two-dimensional square lattice, the half-filled Holstein model predicts the emergence of a CDW phase at any value of the electron-phonon interaction λ [23]. In the presence of an additional on-site electron-electron repulsion U ,

the system can exhibit dominant AFM or CDW correlations depending on the relative magnitude of U and λ [24,25]. Interestingly, there are indications of an intermediate metallic phase between the AFM and CDW phases [26–29], as well as other exotic regimes [30].

For the two-dimensional (2D) square lattice SSH model at half filling, it was shown [31] that a finite critical electron-phonon interaction λ_c is needed to establish the bond-order-wave (BOW) phase, and weak antiferromagnetism was detected [32,33] for $\lambda < \lambda_c$ despite the absence of U . In the dilute limit, where bipolarons are expected to condense into a superfluid at very high temperatures, AFM is revealed as well in the effective Hamiltonian [34]. The cause of this antiferromagnetism is that, on a given bond, only electrons of different spins can tunnel simultaneously, resulting in a lowering of the energy via the electron-phonon coupling on the bonds and an *increase* in the magnitude of the kinetic energy. In contrast, in the Hubbard model at half filling, AFM order emerges in a two-step process in which U first suppresses doubly occupied sites, and then AFM order occurs due to a small remnant exchange process $J \sim 4t^2/U$. The AFM phase in the Hubbard limit is thereby accompanied by low kinetic energy. This distinction will play a role in a crossover behavior we observe in the Su-Schrieffer-Heeger-Hubbard (SSH) phase diagram.

We study here the rich interplay of BOW and AFM regimes in the SSH model. Crucially, since the phonons couple to the electrons via the kinetic term, particle-hole symmetry is preserved and there is no sign problem (SP) at half filling. This

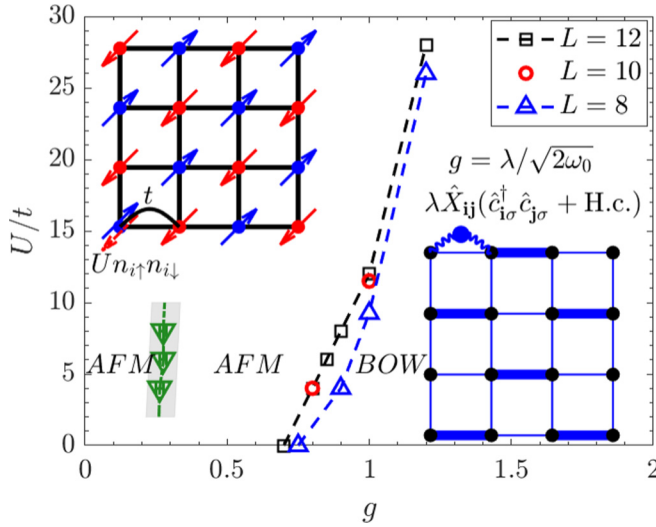


FIG. 1. Phase diagram of the SSH model at half filling. g is the dimensionless electron-phonon coupling constant, and U/t is the Coulomb repulsion strength. A dotted (green) line shows the location of a crossover in the nature of the AFM. $\beta = 16$ ensures the system is close to the ground state for all three lattice sizes. The AFM-BOW transitions for $L = 10, 12$ coincide, indicating negligible finite size effects. The insets show schematically the AFM and BOW phases.

allows us to use determinant quantum Monte Carlo (DQMC) to study systems up to 12×12 in size and at very low temperature. This contrasts with the Hubbard-Holstein model, where the SP precludes crossing the CDW-AFM phase boundary [29]. Our resulting phase diagram (Fig. 1) exposes phases of long-range AFM and BOW order. Prior to our work, only the quantum critical point along the $U = 0$ axis (the SSH Hamiltonian) had been determined [31]. A central observation of this Letter is that there are, within the AFM phase, distinct regimes at small and intermediate electron-phonon coupling λ . The AFM structure factor, double occupancy, and kinetic energy remain almost constant for small λ . However, for larger λ these quantities show a marked dependence on λ . As a consequence, we will argue that the competition between λ and U results not only in the expected AFM-BOW transition, but also in a different crossover *within* the AFM phase. This crossover is clearly signaled in the AFM correlations themselves, and also in the double occupancy, kinetic energy, and pairing structure factors. These changes result from competition of the localizing effect of the Hubbard term and the quantum fluctuations favored by the SSH term, although they both can lead to AFM.

Model and method. We study the square lattice optical SSH model, where the electronic hopping is modulated by an electron-phonon interaction and an on-site Coulomb repulsion is present. The Hamiltonian is

$$\begin{aligned} \mathcal{H} = & -t \sum_{(i,j),\sigma} (1 - \lambda \hat{X}_{ij}) (\hat{c}_{i\sigma}^\dagger \hat{c}_{j\sigma} + \text{H.c.}) - \mu \sum_{i,\sigma} \hat{n}_{i\sigma} \\ & + \sum_{(i,j)} \left(\frac{1}{2M} \hat{p}_{ij}^2 + \frac{M}{2} \omega_0^2 \hat{X}_{ij}^2 \right) \\ & + U \sum_i \left(\hat{n}_{i\uparrow} - \frac{1}{2} \right) \left(\hat{n}_{i\downarrow} - \frac{1}{2} \right), \end{aligned} \quad (1)$$

where $\hat{c}_{i\sigma}$ ($\hat{c}_{i\sigma}^\dagger$) destroys (creates) an electron of spin $\sigma = \uparrow, \downarrow$ on site i , μ is the electron chemical potential, M is the phonon mass, and ω_0 the oscillation frequency. The bond phonon displacement operator \hat{X}_{ij} connects nearest-neighbor sites (i, j) ; its conjugate bond momentum is \hat{P}_{ij} . In the following, the magnitude of electron-phonon coupling is given by the dimensionless parameter $g = \lambda / \sqrt{2M\omega_0/\hbar}$, so that the coupling term is $t g (\hat{b}_{ij} + \hat{b}_{ij}^\dagger) (\hat{c}_{i\sigma}^\dagger \hat{c}_{j\sigma} + \text{H.c.})$. The on-site Coulomb repulsion is U/t , and $\hat{n}_{i\sigma} = \hat{c}_{i\sigma}^\dagger \hat{c}_{i\sigma}$ is the number operator on site i . We work in units for which $\hbar = t = M = 1$ and fix $\omega_0 = 1$.

The Hubbard-Stratonovich (HS) transformation is used in DQMC [6,23,35,36], to express the quartic Coulomb interaction in quadratic form [37,38]. The fermions are integrated out, yielding a determinant of a matrix that has the dimension of the number of spatial sites N . The entries of the matrix depend on the HS and phonon fields. We focus on half filling ($\mu = 0$), which does not present a SP, and work with $\beta = L_\tau \Delta\tau = 16$, where $L_\tau \sim 320$ is the number of imaginary slices, and $\Delta\tau$ is the imaginary time step. This β is sufficiently large to access the ground state of the SSH model on the lattice sizes under investigation here [31].

To characterize the emerging phases, we calculate the average kinetic energy in the x and y directions, $\langle K_{x(y)} \rangle = \langle \hat{c}_{i,\sigma}^\dagger \hat{c}_{i+\hat{x}(y),\sigma} + \text{H.c.} \rangle$, and the average phonon displacement in the x and y directions $\langle X_{x(y)} \rangle$. These give insight into the broken x - y symmetry in the BOW phase. We also study the antiferromagnetic, $\langle S_i^x S_{i+r}^x \rangle$, and the bond-order correlation functions, $\langle K_{x(y)}(i) K_{x(y)}(i+r) \rangle$. Their Fourier transforms, S_{AFM} and $S_{K_{x(y)}}$, are respectively the AFM and BOW structure factors. In addition, we examine the double occupancy, $D = \langle \hat{n}_{i\uparrow} \hat{n}_{i\downarrow} \rangle$, and the total kinetic energy $\langle K \rangle = \langle K_x \rangle + \langle K_y \rangle$, which provide additional important insight.

Results. It is well known [39,40] that, at half filling, the square lattice Hubbard model, Eq. (1) with $\lambda = 0$, exhibits an AFM phase for any $U > 0$. Similarly, it was recently established [32,33] that the two-dimensional SSH model, Eq. (1) with $U = 0$, exhibits, at low temperature, an AFM phase for small λ and a BOW [31] when λ exceeds a critical value. Here, we address the unknown structure of the phase diagram in the $(g, U/t)$ plane.

To this end, we determine the phase boundaries with vertical and horizontal cuts, i.e., by fixing g (U/t) and studying the behavior of the system as U/t (g) is changed. The AFM and BOW phases are revealed by their respective structure factors, S_{AFM} and $S_{K_x}(\pi, \pi)$. For low temperature and large systems, we start simulations with a phonon configuration that favors the BOW phase in the x direction (bottom right inset of Fig. 1) because this structure is found to melt rapidly in the AFM phase, but takes a long equilibration time to form. In principle, if we start with a random configuration, all of the four degenerate BOW ground states can be reached if we run long enough, as discussed in Ref. [31]. But in practice, tunneling between these symmetry-equivalent ground states is rare on the very large space-time lattices we study here, much as occurs in the thermodynamic limit for an experimental measurement. A “standard,” and well-documented, numerical way to address this issue is to begin with an ordered pattern conforming to one of the degenerate ground states. The technique works well in part because in the disordered phase

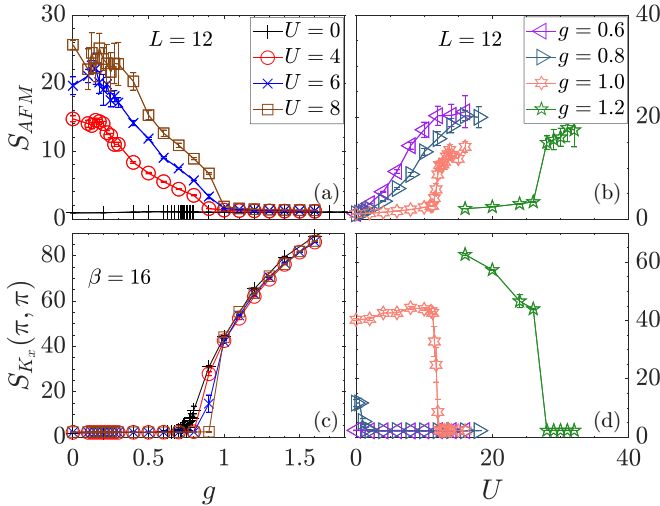


FIG. 2. DQMC results of the AFM (BOW) structure factor $S_{\text{AFM}} [S_{K_x}(\pi, \pi)]$ for horizontal (left) and vertical (right) cuts in the phase diagram. In the AFM phase, S_{AFM} is finite and $S_{K_x}(\pi, \pi)$ is negligible. In the BOW phase, S_{AFM} is negligible and $S_{K_x}(\pi, \pi)$ is finite.

the system relatively easily relaxes from the initial ordered pattern, so that it does not affect the determination of the critical point and only, trivially, selects out a particular ordered phase. We measure $S_{K_x(y)}(k_x, k_y)$ for all momenta and observe a peak only at $S_{K_x}(\pi, \pi)$ when the system is in the BOW phase [see more details in the Supplemental Material [41] (see also Refs. [32,33,42,43] therein)]. A comparison of data for $L = 10, 12$ indicates negligible finite size effects.

Figures 2(a) and 2(c) show the structure factors versus the dimensionless g for several fixed values of U/t . For $U/t = 4, 6, 8$ the system is a Hubbard AFM for $g = 0$, and remains AFM as g increases up to a critical value, $g_c(U/t)$. For $g < g_c$, S_{K_x} is small, indicating the absence of BOW. S_{K_x} then rises rapidly upon entry into the BOW phase at $g > g_c$.

The behavior of the AFM structure factor S_{AFM} is more subtle. It is nonzero for $g < g_c$, but there is an appreciable change in behavior well *before* its value drops precipitously: S_{AFM} is initially constant for small g [Fig. 2(a)], but starts decreasing at $g_* \approx 0.2$. A finite size scaling analysis [41] shows that AFM regions exhibit true long-range order on both sides of g_* . The difference between these two AFM regions, inferred from the kinetic energy and double occupancy will be discussed below. Indeed, since data for structure factors are more noisy than local correlation functions, these complementary observables will present additional compelling evidence for the crossover behavior at g_* .

Returning to the AFM-BOW transition with increasing g , we see [Fig. 2(a)] that when S_{AFM} drops, S_{K_x} becomes nonzero. This occurs at $g_c \sim 1$ for $L = 12$. In Figs. 2(b) and 2(d) we show the same quantities as Figs. 2(a) and 2(c) but now g is fixed and U/t varies. For $g = 0.6$, S_{K_x} is small for all U/t while S_{AFM} increases smoothly as U/t increases. For this value of g the system is always AFM. For $g \geq 0.8$, S_{AFM} is very small (essentially zero) while S_{K_x} is large up to a g -dependent critical value $U_c(g)$, indicating that the system is in the BOW phase [31]. At $U_c(g)$, there is a first-order transition

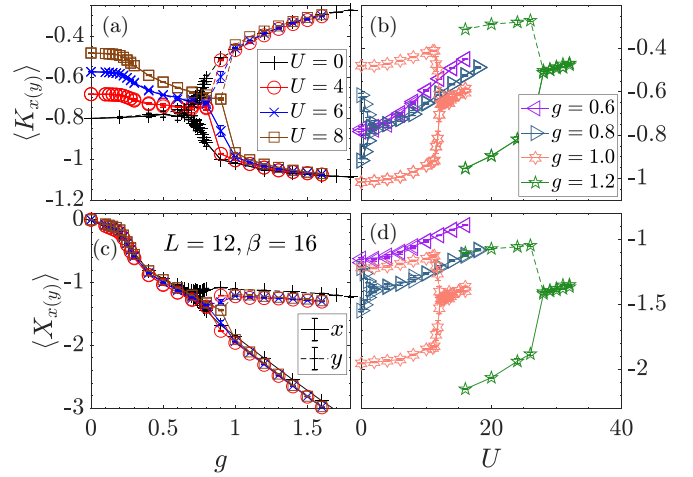


FIG. 3. DQMC results of average kinetic energy $\langle K_{x(y)} \rangle$ and average phonon displacement $\langle X_{x(y)} \rangle$ in x and y directions for horizontal (left) and vertical (right) cuts in the phase diagram.

from the BOW to the AFM phase, with clear discontinuous jumps in the order parameters. This first-order character is also observed for the larger U values in the horizontal cuts (sweeping g at fixed U) in Figs. 2(a) and 2(c).

As shown in Ref. [31], the BOW has (π, π) ordering vector either in x or in y with two sublattice possibilities in each direction, resulting in the Z_4 symmetry breaking (in the thermodynamic limit). We now focus on this symmetry breaking as the system leaves the AFM phase and enters the BOW phase. In the AFM phase, the average kinetic energy and phonon displacement in the x and y directions are equal. In the BOW phase, the average kinetic energy and phonon displacement which align with the BOW direction increase in magnitude. We show in Fig. 3 the behavior of these quantities for the same parameters as in Fig. 2. In Figs. 3(a) and 3(c), the x - y symmetry is preserved in the AFM phase, $g < g_c(U)$, and broken immediately when the system enters the BOW phase. This is clearly seen in the bifurcation in $K_{x(y)}$ and $X_{x(y)}$ at g_c . As the on-site interaction becomes stronger, the electron-phonon coupling strength required to establish the BOW phase becomes larger.

In Figs. 3(b) and 3(d), for constant g , the x - y symmetry is broken for $U < U_c(g)$, $g \geq 0.8$, and restored immediately when the system exits the BOW and enters the AFM phase at $U_c(g)$. For $g = 0.6$, the system is never in the BOW phase for all U and therefore the x - y symmetry is always preserved. The values of $g_c(U)$ and $U_c(g)$ obtained in Figs. 2 and 3 are in close agreement. We remark that, as observed in both figures, a small increase in g (i.e., from 1.0 to 1.2) leads to significant changes of U_c (i.e., from 12 to 26). Putting these cuts at constant g and U together yields the phase diagram shown in Fig. 1.

We now focus on the two AFM regions (separated by the vertical dotted line in Fig. 1) for which S_{AFM} provided initial evidence. We recall that for $g = 0$, the system is in the Hubbard AFM phase for any $U > 0$, while for $U = 0$, the system is in the SSH AFM phase [32,33] for small g . The SSH AFM at $U = 0$ clearly has a different mechanism from

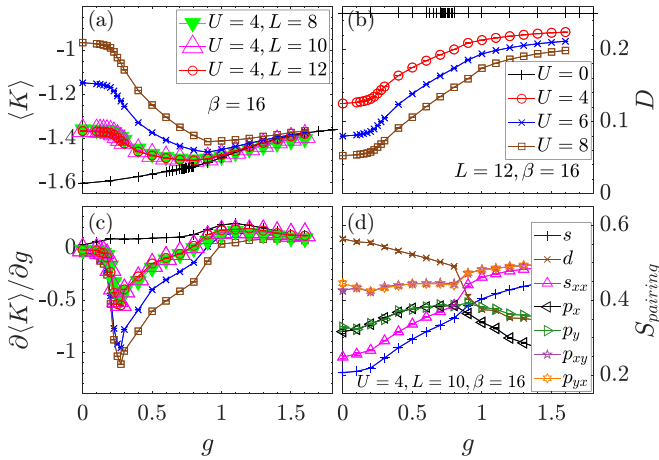


FIG. 4. (a) Average kinetic energy. (b) Double occupancy for different U and fixed lattice size $L = 12$. (c) Derivative of the kinetic energy with respect to g . The legends in (a) and (b) explain the symbols in (a)–(c). (d) Pairing structure factors at fixed $U = 4$ and $L = 10$.

the traditional two-step Hubbard model process of moment formation at energy scale U , followed by moment ordering at energy scale $J \sim 4t^2/U$. A close analysis of Figs. 3(a) and 3(c) shows that both $\langle K_{x(y)} \rangle$ and $\langle X_{x(y)} \rangle$ remain almost constant for $g \lesssim 0.2$ and then increase in magnitude for $g > 0.2$. Similarly, the AFM structure factor in Fig. 2(a) is approximately constant for $g \lesssim 0.2$ and decreases for larger values of g .

In Fig. 4(a), we show the average kinetic energy as a function of g for several values of U . $\langle K \rangle$ clearly exhibits a change of behavior at $g_* \approx 0.2$, supporting what is seen in Fig. 2 for S_{AFM} . This is captured even more effectively in Fig. 4(c), which shows a sharp peak at $g \sim 0.275$ in $\partial \langle K \rangle / \partial g$ vs g . A comparison between $\langle K \rangle$ given in this SSHH Hamiltonian and in an (approximate) “effective” Hubbard model [41] gives more insight on this crossover. Figure 4(b) shows the double occupancy D which increases in value for $g \gtrsim 0.2$. This behavior (larger kinetic energy and double occupancy) indicates that the system has left the “large U ” Hubbard AFM, where both quantities are suppressed, and entered an AFM region strongly influenced by the SSH electron-phonon coupling, where quantum fluctuations are large. Going from one of these AFM regions to the other is a crossover, not a phase transition. Nevertheless, there is a clear signature in the increased quantum fluctuations.

Since the pure SSH Hamiltonian preserves $O(4)$ symmetry, and an AFM/CDW/SC degenerate ground state is expected in the adiabatic limit [32,33], it is useful to examine the superconducting structure factor S_{pairing} , the spatial sums of the real-space correlations $\langle \Delta_\alpha(i+r)\Delta_\alpha^\dagger(i) \rangle$ with standard conventions $\Delta_s^\dagger(i) = c_{i\uparrow}^\dagger c_{i\downarrow}^\dagger$, $\Delta_d^\dagger(i) = c_{i\uparrow}^\dagger \frac{1}{2}(c_{i+x\downarrow}^\dagger - c_{i+y\downarrow}^\dagger + c_{i-x\downarrow}^\dagger - c_{i-y\downarrow}^\dagger)$, etc. [44]. These are shown in Fig. 4(d). Similar changes are observed at the crossover. A bifurcation in pairing with p_x and p_y symmetry, as well as the sharp change in d , and s_{xx} pair form factors, at $g_c \sim 0.9$ also signal the AFM-BOW phase transition. An interesting, and intuitively reasonable, observation is that a BOW pattern formed along the x or y direction of the square lattice increases pairing

along plaquette diagonals (p_{xy} , p_{yx} , and s_{xx}), but competes with pairing channels which are also aligned directly along the bonds (d , p_x , p_y).

Conclusions. In this Letter, we used DQMC simulations to map out the phase diagram of the single-orbital square lattice optical SSHH model. Our work fills in the full two-dimensional phase diagram in the plane of positive U and g , hitherto only investigated along the $U = 0$ and $g = 0$ axes. The phase diagram is characterized by BOW and AFM phases. At larger electron-phonon coupling strength, the x - y symmetry is spontaneously broken and the system develops a BOW with a (π, π) order. Given the different broken symmetries in the BOW and AFM phases, and the sharp increase of the BOW structure factor, the results indicate a first-order transition between these two phases. The most salient feature is that the ground state phase transition is much more sensitive to changes in electron-phonon coupling compared to variations in the Coulomb repulsion. We interpret this as the result of the lack of a direct competition between the two ordered phases. In the Hubbard-Holstein model, U suppresses double occupancy while the Holstein g enhances it. Thus the two interactions always conflict: They want the most fundamental structure, the site occupations, to behave completely differently, yielding $U_c \sim g^2$ (at $\omega_0 = 1$). No such competition appears in the SSHH model. Indeed, both interactions individually give rise to AFM order, leading to somewhat cooperative tendencies. We thus argue that this is why adding U does not significantly inhibit the formation of the BOW phase by the SSH phonons, leading to a near vertical phase boundary.

In the AFM region, for small electron-phonon coupling g , all the quantities that we analyzed, e.g., the AFM structure factor, kinetic energy, phonon displacement, and double occupancy, remain approximately constant. For $g \gtrsim 0.2$, the double occupancy and the magnitude of the kinetic energy start increasing, while the AFM structure factor decreases. This occurs even though the system still possesses true long-range AFM order as demonstrated by a finite size scaling analysis [41]. This is due to the fact that the Hubbard AFM and the SSH AFM mechanisms are different [32,33]. This insight into the physics of the SSH-Hubbard Hamiltonian can be thought of as analogous to the well-established crossover from a Slater insulator to Mott-Hubbard insulator and from itinerant AFM to Heisenberg AFM with increasing U in the Hubbard model ($g = 0$) [40,45,46]. We focused here on intermediate to strong coupling, i.e., U exceeding half the bandwidth $W = 8t$ and $\omega_0 = t$. Further investigation of the effect of ω_0 on the crossover is of interest.

Individually, the Hubbard and SSH Hamiltonians exhibit a rich panoply of phenomena when doped away from half filling. The interaction U leads to a complex mixture of pseudogap physics, strange metal behavior, stripe order, and d -wave pairing when doped. The SSH model hosts polarons in the dilute limit which can bind to bipolarons and condense into superconducting phases. Other phases of matter are thus likely to emerge from the study of regimes of the SSHH Hamiltonian away from half filling. Work in this direction has already begun as shown in Ref. [47].

Note Added. We have recently become aware of the manuscript [48] which reports closely related work.

Acknowledgments. We acknowledge fruitful discussions with W.-T. Chiu and B. Cohen-Stead. C.H.F. and R.S. are supported by Grant No. DOE DE-SC0014671 funded by the U.S. Department of Energy, Office of Science. D.P. acknowledges support from the Singapore Min-

istry of Education, Singapore Academic Research Fund Tier-II (Project No. MOE2018-T2-2-142). The computational work for this Letter was performed on resources of the National Supercomputing Centre, Singapore (NSCC) [49].

-
- [1] J. Hubbard, Electron correlations in narrow energy bands, *Proc. R. Soc. London, Ser. A* **276**, 238 (1963).
- [2] A. Georges, G. Kotliar, W. Krauth, and M. J. Rozenberg, Dynamical mean-field theory of strongly correlated fermion systems and the limit of infinite dimensions, *Rev. Mod. Phys.* **68**, 13 (1996).
- [3] P. A. Lee, N. Nagaosa, and X.-G. Wen, Doping a Mott insulator: Physics of high-temperature superconductivity, *Rev. Mod. Phys.* **78**, 17 (2006).
- [4] T. Holstein, Studies of polaron motion: Part I. The molecular-crystal model, *Ann. Phys.* **8**, 325 (1959).
- [5] W. P. Su, J. R. Schrieffer, and A. J. Heeger, Solitons in Polyacetylene, *Phys. Rev. Lett.* **42**, 1698 (1979).
- [6] R. M. Noack, D. J. Scalapino, and R. T. Scalettar, Charge-Density-Wave and Pairing Susceptibilities in a Two-Dimensional Electron-Phonon Model, *Phys. Rev. Lett.* **66**, 778 (1991).
- [7] M. Vekić, R. M. Noack, and S. R. White, Charge-density waves versus superconductivity in the Holstein model with next-nearest-neighbor hopping, *Phys. Rev. B* **46**, 271 (1992).
- [8] Y.-X. Zhang, W.-T. Chiu, N. C. Costa, G. G. Batrouni, and R. T. Scalettar, Charge Order in the Holstein Model on a Honeycomb Lattice, *Phys. Rev. Lett.* **122**, 077602 (2019).
- [9] C. Chen, X. Y. Xu, Z. Y. Meng, and M. Hohenadler, Charge-Density-Wave Transitions of Dirac Fermions Coupled to Phonons, *Phys. Rev. Lett.* **122**, 077601 (2019).
- [10] C. Feng, H. Guo, and R. T. Scalettar, Charge density waves on a half-filled decorated honeycomb lattice, *Phys. Rev. B* **101**, 205103 (2020).
- [11] M. Weber and M. Hohenadler, Two-dimensional Holstein-Hubbard model: Critical temperature, Ising universality, and bipolaron liquid, *Phys. Rev. B* **98**, 085405 (2018).
- [12] B. Cohen-Stead, N. C. Costa, E. Khatami, and R. T. Scalettar, Effect of strain on charge density wave order in the Holstein model, *Phys. Rev. B* **100**, 045125 (2019).
- [13] Z.-X. Li, M. L. Cohen, and D.-H. Lee, Enhancement of superconductivity by frustrating the charge order, *Phys. Rev. B* **100**, 245105 (2019).
- [14] C. Feng and R. T. Scalettar, Interplay of flat electronic bands with Holstein phonons, *Phys. Rev. B* **102**, 235152 (2020).
- [15] B. Nosarzewski, E. W. Huang, P. M. Dee, I. Esterlis, B. Moritz, S. A. Kivelson, S. Johnston, and T. P. Devereaux, Superconductivity, charge density waves, and bipolarons in the Holstein model, *Phys. Rev. B* **103**, 235156 (2021).
- [16] B. Xiao, N. C. Costa, E. Khatami, G. G. Batrouni, and R. T. Scalettar, Charge density wave and superconductivity in the disordered Holstein model, *Phys. Rev. B* **103**, L060501 (2021).
- [17] O. Bradley, G. G. Batrouni, and R. T. Scalettar, Superconductivity and charge density wave order in the two-dimensional Holstein model, *Phys. Rev. B* **103**, 235104 (2021).
- [18] P. M. Dee, J. Coulter, K. G. Kleiner, and S. Johnston, Relative importance of nonlinear electron-phonon coupling and vertex corrections in the Holstein model, *Commun. Phys.* **3**, 145 (2020).
- [19] H. G. Keiss, *Conjugated Conducting Polymers*, Springer Series in Solid-State Sciences Vol. 102 (Springer, Berlin, 1992).
- [20] T. Ishiguro and K. Yamaji, *Organic Superconductors* (Springer, Berlin, 1990).
- [21] H. Toftlund and O. Simonsen, Preparation and structure of a new kind of an extended partially oxidized linear-chain compound: Catena-(μ -bromo)bis((1*R*, 2*R*)-cyclohexanediamine)nickel(2.77) bromide, *Inorg. Chem.* **23**, 4261 (1984).
- [22] M. Hase, I. Terasaki, and K. Uchinokura, Observation of the Spin-Peierls Transition in Linear Cu^{2+} (Spin-1/2) Chains in an Inorganic Compound CuGeO_3 , *Phys. Rev. Lett.* **70**, 3651 (1993).
- [23] R. T. Scalettar, N. E. Bickers, and D. J. Scalapino, Competition of pairing and Peierls-charge-density-wave correlations in a two-dimensional electron-phonon model, *Phys. Rev. B* **40**, 197 (1989).
- [24] W. Koller, D. Meyer, Y. Ōno, and A. C. Hewson, First- and second-order phase transitions in the Holstein-Hubbard model, *Europhys. Lett.* **66**, 559 (2004).
- [25] P. Werner and A. J. Millis, Efficient Dynamical Mean Field Simulation of the Holstein-Hubbard Model, *Phys. Rev. Lett.* **99**, 146404 (2007).
- [26] H. Fehske, G. Hager, and E. Jeckelmann, Metallicity in the half-filled Holstein-Hubbard model, *Europhys. Lett.* **84**, 57001 (2008).
- [27] S. Johnston, E. A. Nowadnick, Y. F. Kung, B. Moritz, R. T. Scalettar, and T. P. Devereaux, Determinant quantum Monte Carlo study of the two-dimensional single-band Hubbard-Holstein model, *Phys. Rev. B* **87**, 235133 (2013).
- [28] Y. Wang, I. Esterlis, T. Shi, J. I. Cirac, and E. Demler, Zero-temperature phases of the two-dimensional Hubbard-Holstein model: A non-Gaussian exact diagonalization study, *Phys. Rev. Research* **2**, 043258 (2020).
- [29] N. C. Costa, K. Seki, S. Yunoki, and S. Sorella, Phase diagram of the two-dimensional Hubbard-Holstein model, *Commun. Phys.* **3**, 80 (2020).
- [30] Z. Han, S. A. Kivelson, and H. Yao, Strong Coupling Limit of the Holstein-Hubbard Model, *Phys. Rev. Lett.* **125**, 167001 (2020).
- [31] B. Xing, W.-T. Chiu, D. Poletti, R. T. Scalettar, and G. Batrouni, Quantum Monte Carlo Simulations of the 2D Su-Schrieffer-Heeger Model, *Phys. Rev. Lett.* **126**, 017601 (2021).
- [32] X. Cai, Z.-X. Li, and H. Yao, Antiferromagnetism Induced by Bond Su-Schrieffer-Heeger Electron-Phonon Coupling: A Quantum Monte Carlo Study, *Phys. Rev. Lett.* **127**, 247203 (2021).

- [33] A. Götz, S. Beyl, M. Hohenadler, and F. F. Assaad, Valence-bond solid to antiferromagnet transition in the two-dimensional Su-Schrieffer-Heeger model by Langevin dynamics, *Phys. Rev. B* **105**, 085151 (2022).
- [34] J. Sous, M. Chakraborty, R. V. Krems, and M. Berciu, Light Bipolarons Stabilized by Peierls Electron-Phonon Coupling, *Phys. Rev. Lett.* **121**, 247001 (2018).
- [35] R. Blankenbecler, D. J. Scalapino, and R. L. Sugar, Monte Carlo calculations of coupled boson-fermion systems. I, *Phys. Rev. D* **24**, 2278 (1981).
- [36] G. G. Batrouni and R. T. Scalettar, Langevin simulations of a long-range electron-phonon model, *Phys. Rev. B* **99**, 035114 (2019).
- [37] R. L. Stratonovich, On a method of calculating quantum distribution functions, *Sov. Phys. Dokl.* **2**, 416 (1957).
- [38] J. Hubbard, Calculation of Partition Functions, *Phys. Rev. Lett.* **3**, 77 (1959).
- [39] J. E. Hirsch and S. Tang, Antiferromagnetism in the Two-Dimensional Hubbard Model, *Phys. Rev. Lett.* **62**, 591 (1989).
- [40] S. R. White, D. J. Scalapino, R. L. Sugar, E. Y. Loh, J. E. Gubernatis, and R. T. Scalettar, Numerical study of the two-dimensional Hubbard model, *Phys. Rev. B* **40**, 506 (1989).
- [41] See Supplemental Material at <http://link.aps.org/supplemental/10.1103/PhysRevB.106.L081114> for (a) An approximate treatment of the SSHH model in terms of a pure Hubbard Hamiltonian with a renormalized U_{eff} ; (b) The BOW structure factor with $U = 4$, $g = 1.5$; $U = 4, 15$ at $g = 1.0$ for $\beta = 16$, $L = 12$ system; (c) Scaling of the antiferromagnetic structure factor; (d) RG-invariant correlation ratio of structure factors; and, finally, (e) Structure factors at several different temperatures.
- [42] I. G. Lang and Yu. A. Firsov, Kinetic theory of semiconductors with low mobility, *J. Exptl. Theor. Phys. (U.S.S.R.)* **43**, 1843 (1962) [*Sov. Phys. JETP* **16**, 1301 (1963)].
- [43] D. Rossini and E. Vicari, Coherent and dissipative dynamics at quantum phase transitions, *Phys. Rep.* **936**, 1 (2021).
- [44] S. R. White, D. J. Scalapino, R. L. Sugar, N. E. Bickers, and R. T. Scalettar, Attractive and repulsive pairing interaction vertices for the two-dimensional Hubbard model, *Phys. Rev. B* **39**, 839(R) (1989).
- [45] T. Pruschke and R. Zitzler, From Slater to Mott–Heisenberg physics: The antiferromagnetic phase of the Hubbard model, *J. Phys.: Condens. Matter* **15**, 7867 (2003).
- [46] M. Raczkowski, F. F. Assaad, and M. Imada, Local moments versus itinerant antiferromagnetism: Magnetic phase diagram and spectral properties of the anisotropic square lattice Hubbard model, *Phys. Rev. B* **103**, 125137 (2021).
- [47] C. Zhang, N. V. Prokof'ev, and B. V. Svistunov, Bond bipolarons: Sign-free Monte Carlo approach, *Phys. Rev. B* **105**, L020501 (2022).
- [48] X. Cai, Z.-X. Li, and H. Yao, Robustness of antiferromagnetism in the Su-Schrieffer-Heeger Hubbard model, *Phys. Rev. B* **106**, L081115 (2022).
- [49] <https://www.nscg.sg>.